J. Plasma Physics (1998), *vol.* 60, *part* 1, *pp.* 3–15. Printed in the United Kingdom

© 1998 Cambridge University Press

Experiments on speed-enhanced neutron yield from a small plasma focus

A. SERBAN and S. LEE

Nanyang Technological University, National Institute of Education,
469 Bukit Timah Road, 259756 Singapore

(Received 28 March 1996 and in revised form 15 October 1997)

In order to operate a plasma focus at high axial sheath velocities, the geometry of the inner electrode (anode) of a 3 kJ Mather-type device was modified. Double-stage stepped-anode configurations were tested with the speed-enhanced region sufficiently long for a significant increase in speed but not long enough to allow the development of force-field flow-field separation at the end of the axial phase. Peak axial speeds up to 15 cm μs^{-1} were achieved. The neutron and soft X-ray productions were found to be sheath-velocity-dependent. A new scaling law for the non-beam component of the neutron yield is proposed.

1. Introduction

The most important areas for developing immediate practical applications using a plasma focus are those that employ the device as a pulsed radiation (i.e. neutron or soft X-ray) source. Therefore special attention has to be given to studies of radiation mechanisms. Based on these studies, new methods for enhancing the radiation yield could be developed.

An analysis of data for Mather-type plasma-focus devices for their wide range of sizes, with the energy stored in the driver ranging from 1 kJ to 1 MJ (Haines 1982; Kies 1988; Herold 1990; Conrads 1992; Bernard *et al.* 1994) shows the following experimentally observed features.

(i) The total neutron yield scales with the focus current as $Y_n \propto I^4$.

(ii) Plasma focus devices can be optimized either for large X-ray output or for high neutron production.

(iii) For neutron-optimized operating conditions, the following properties are seen.

  (*a*) They all have the same limited peak axial sheath velocity v_{axial} of 10 cm μs^{-1} and radial on-axis collapse speed of 25 cm μs^{-1}; this fixes the forward shock temperature on axis at 1.4×10^6 K, and the on-axis reflected-shock temperature at 3.6×10^6 K. Further compression brings the temperature of the gross plasma column to just under 1 keV (Lee 1988, 1990).

  (*b*) They are all driven by a standard value of a drive parameter $(I_p/a)\ \rho_0^{-1/2}$ (i.e. the peak drive current per unit anode radius divided by the square root of the fill density) of $89(\pm 8)$ kA cm^{-1} (Torr D_2)$^{-1/2}$ (Lee and Serban 1996) (for simplicity, the gas density is replaced by pressure and the drive parameter is written as $(I_p/a)\ p^{-1/2}$). This ensures for all machines the same value of the drive magnetic field in the axial phase

https://doi.org/10.1017/S0022377898006771 Published online by Cambridge University Press

and the same compressed energy density in the focus phase, leading to the same high temperature in all devices (Lee 1990, 1994).

(*c*) They all have a maximum density of the pinched plasma in the region of $(1\text{–}5) \times 10^{19}$ cm^{-3} (Lee *et al.* 1988).

(*d*) They all operate in a narrow range of deuterium filling pressures of several torr.

(iv) They have a plasma impedance about 0.3 Ω (Bernard *et al.* 1994).

The neutron scaling law shows that the larger plasma focus devices produce more neutrons. This increased neutron yield appears to be due only to a combination of the larger volume of the focused plasma and the consequent increase in the lifetime of the focused region. Any realistic modelling of the plasma focus will show that each linear dimension of the approximately cylindrical focus or pinch region is proportional to the anode radius (Lee 1983, 1988; Lee and Serban 1996). Since all plasma focus devices are conventionally designed with nearly the same drive parameter, it follows that the volume of the focused or pinched plasma is proportional to I_p^3. The lifetime of plasma confinement is limited by the magnetohydrodynamic transit time. This transit time is a function only of the smallest linear pinch dimension, and hence of I_p, since the energy densities that control the relevant magnetohydrodynamic speeds are practically identical, as discussed above. Combining these scalings of volume and confinement time immediately gives the experimentally observed scaling law $Y_n \propto I^4$.

A good focusing effect is usually obtained in plasma focus experiments when the peak axial sheath velocity is within the limited range of 6–10 cm μs^{-1} and the drive parameter is about 89 kA cm^{-1} (Torr D_2)$^{-1/2}$ (Lee & Serban 1996). The lower speed limit is easily understood in terms of poor coupling of the magnetic piston with the driven plasma layer, indicated by a low magnetic Reynolds number R_m (Lee *et al.* 1991), or in terms of low specific energy (Pouzo *et al.* 1988). For the higher speed limit, it appears that the high R_m leads to an effective separation of the magnetic piston from the plasma layer. The plasma layer then collapses radially, whilst the magnetic piston is still driving axially (Lee 1994). Such a force-field flow-field separation is not conducive to an intense focus. Other possible mechanisms responsible for the upper speed limit are due to

(i) plasma–anode interactions or, more specifically, the ion (and sometimes, electron) current component;

(ii) the development of Rayleigh–Taylor instabilities;

(iii) at high velocities, the mean free path increasing and subsequently the shock becoming diffusive, hence making the drive ineffective.

In the light of these factors, the idea of driving the plasma with speeds exceeding the 'magic' value of 10 cm μs^{-1}, but at the same time trying to overcome the difficulties mentioned above and to achieve good focusing effect, became challenging. Of course, one of the possibilities for increasing the speed is to reduce the gas filling pressure, but in this way one switches from one operating regime to another, and the effects are already known. In fact, a change of pressure is the practical way to optimize a given machine (fixed geometry) to operate in a certain regime.

https://doi.org/10.1017/S0022377898006771 Published online by Cambridge University Press

In our work we studied the performance of a plasma focus driven by peak axial sheath velocities up to 10–15 cm μs^{-1} without changing the gas filling pressure or the charging voltage. Our first objective was to characterize the focus operating with the standard electrode geometry and to correlate various plasma parameters like thickness and inclination of the sheath, size, location and temperature of the pinch, development of macroinstabilities, X-ray production, and neutron yield.

Secondly – and this was the new element introduced by our experimental work – in order to increase the drive parameter and at the same time to limit the force-field flow-field separation, we used a stepped anode structure, which we call a composite anode (see Fig. 1). The first part of the axial phase uses a regular anode designed for the standard $(I_p/a)\, p^{-1/2}$, but shorter than required to match the discharge peak. This regular anode is attached to a stepped-down anode of smaller radius. This is the speed-enhanced section with increased value of $(I_p/a)\, p^{-1/2}$, which should be long enough to increase the speed significantly above 10 cm μs^{-1}, but short enough to limit the force-field flow-field separation.

Our hypothesis is that a good focusing effect occurring at higher speeds implies the achievement of higher temperatures of the pinched column. This will automatically lead to an enhanced radiation output. A possible explanation of this effect is based on an idea proposed by Lee (1988, 1994). He suggested that removing the speed limitation would ultimately result in a vastly improved scaling law $Y_n \propto I^8$, which could enhance the prospects of the plasma focus as a fusion contender.

Operating the focus at higher velocities, and hence higher temperatures, the thermonuclear component Y_{th} of the total neutron production is enhanced. It can easily be shown that $Y_{\mathrm{th}} \propto I^4 v_{\mathrm{axial}}^4$, and the beam–target component of the neutron yield $Y_{\mathrm{bt}} \propto I^{4.5} v_{\mathrm{axial}}^{-1.5}$.

The total neutron yield is $Y_n = Y_{\mathrm{th}} + Y_{\mathrm{bt}}$. If the experiments do not limit the speed of operation then Y_{th} will increase above the I^4 scaling whilst Y_{bt} will have a scaling law poorer than $I^{4.5}$. In the limit keeping the anode radius constant whilst increasing the current,

$$Y_{\mathrm{th}} \propto I^8, \qquad Y_{\mathrm{bt}} \propto I^3.$$

The following conclusions may be drawn from such an analysis: operating at higher speeds, above 10 cm μs^{-1}, should

(i) increase the thermonuclear component of the neutron yield preferentially to the beam–target component;

(ii) make the scaling law more favourable than I^4, with the ultimate, most favourable scaling law being $Y \propto I^8$ (Lee 1994; Lee and Serban 1994).

In view of such analysis, a further objective of our work was to obtain indications regarding how neutron production scales with speed.

2. Apparatus

The evolution, dynamics, and discharge characteristics of a 3 kJ Mather-type plasma focus device were studied using two different electrode configurations (see Fig. 1). The outer electrode used as cathode was not modified. The two basic kinds of geometries of the anode were:

https://doi.org/10.1017/S0022377898006771 Published online by Cambridge University Press

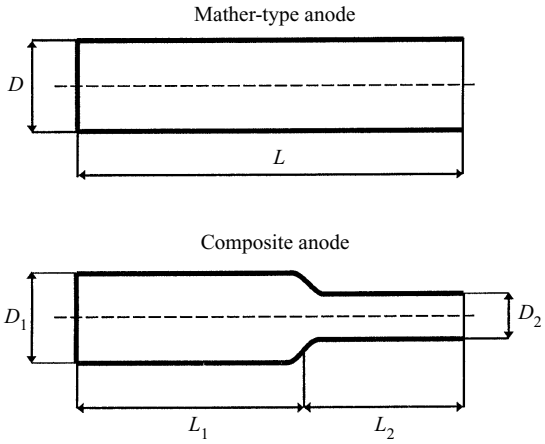


Figure 1. Anode configurations: one-piece Mather-type anode (top) and stepped-down composite anode (bottom).

Table 1. One-piece Mather-type anode configurations (OPA).

Name	L (mm)	D (mm)
SPF-165/19	165	19
OPA-185/15	185	15
OPA-180/17	180	17
OPA-175/17.5	175	17.5

Table 2. Composite-anode configurations (CCA). All dimensions are in mm.

Name	L_1	D_1	L_2	D_2
CCA-120/19+50/15	120	19	50	15
CCA-103/19+70/15	103	19	70	15
CCA-93/19+80/15	93	19	80	15
CCA-90/19+100/15	90	19	100	15
CCA-95/19+90/14	95	19	90	14
CCA-65/19+120/45	65	19	120	15
CCA-45/19+140/15	45	19	140	15

(i) a one-piece Mather-type anode (OPA; Fig. 1 and Table 1);

(ii) a stepped anode called a composite anode (CCA; Fig. 1 and Table 2).

The first part of this stepped anode was a regular Mather-type anode designed for our plasma focus device, but cut shorter than required to match the discharge peak. The diameter of the first part of the anode was 19 mm (see Table 2). This corresponded to the diameter of the original anode of the focus device designed for operating at 15 kV. Thus we do not change the conditions for the first part of the discharge, i.e. the breakdown, lift-off and axial propagation phases. This part was attached to a stepped-down anode of smaller radius. This second stage of the anode is referred to as the speed-enhanced section, which we attempt to adjust in length and diameter. All the anodes used were hollow at the open end.

https://doi.org/10.1017/S0022377898006771 Published online by Cambridge University Press

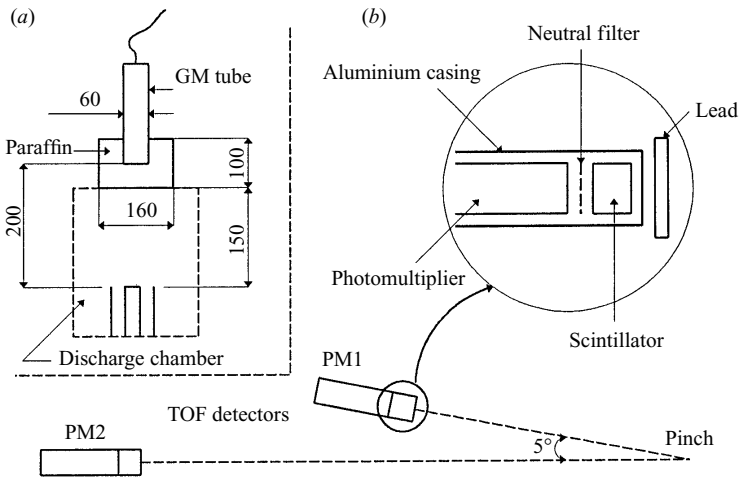


Figure 2. Schematic of experimental arrangements for neutron measurements: (*a*) neutron yield (all dimensions are in mm); (*b*) time-resolved neutron flux and time-of-flight.

The diagnostic techniques employed include current and voltage measurements, shadowgraphic investigations, time-resolved neutron measurements and total neutron yield, and axial sheath velocity measurements. The plasma electron temperature during the pinch phase was determined using the filter ratio method.

Measurements of the total neutron yield were carried out using the indium foil activation technique. A schematic of the experimental set-up is illustrated in Fig. 2(*a*). The calibration factor of our system (BICRON Labtech Analyzer with GM tube) was 3.4×10^5 neutrons/count. Time-resolved neutron flux measurements were carried out with two time-of-flight (TOF) detectors. A schematic diagram of the experimental arrangement is shown in Fig. 2(*b*).

Each TOF detector consists of a plastic scintillator NE 102A of 50 mm diameter and 40 mm thickness coupled to a photomultiplier EMI 9813B. The plastic scintillator was wrapped in aluminium foil except for the side facing the window of the photomultiplier. Dow Corning 200 silicon grease was used between the plastic scintillator and the window of the photomultiplier for proper optical coupling.

Assuming a typical plasma-focus discharge producing an average yield of 10^8 neutrons/shot isotropically, the estimated numbers of neutrons reaching the TOF detectors (placed radially at $3.6(\pm 0.04)$ m and $6.1(\pm 0.04)$ m respectively) were approximately 1150 and 400 respectively. Therefore, in order to obtain output signals (to the oscilloscope) of approximately the same amplitude from both TOF detectors, neutral filters were placed between the plastic scintillators and the windows of the photomultipliers (see Fig. 2*b*).

The TOF detectors were enclosed in aluminium casings. Lead sheets of up to 6 mm thickness were placed in front of the TOF detectors to cut off most of the hard X-rays.

https://doi.org/10.1017/S0022377898006771 Published online by Cambridge University Press

3. Results and discussion

The results of our experiments with basically two types of anode geometries, namely a one-piece anode and a composite or double-stage anode, show that, in terms of radiation output, there are significant differences among the electrode configurations studied. However, for the plasma focus evolution and dynamics, in practice two operating regimes are identified. One corresponds to discharges with single voltage spike. This is an indication of a single compression of the plasma column during the pinch phase. In these cases the neutron output is above the average value for each anode geometry. The other plasma focus regime is associated with multiple voltage spikes, which, in turn, indicate multiple compressions of the pinched column. The neutron productions were generally below the average for each electrode configuration.

The common characteristics of all electrode configurations investigated are as follows.

(i) The neutron-optimized operating pressure is 450 Pa for a charging voltage of 14 kV.

(ii) The neutron output of the plasma focus has a strong dependence on the gas filling pressure: the total neutron production has a pronounced maximum at 450 Pa deuterium; the neutron yield drops relatively sharply with increasing gas pressure, while deteriorating less drastically for decreasing pressures.

(iii) Discharges with high neutron production are always accompanied by low soft X-ray output, but by high emission in the hard X-ray region.

At the same time, correlations of the plasma focus parameters have been made. The purpose was to get a better understanding of the evolution and dynamics of the plasma focus, as well as to benchmark the device for a given electrode configuration and operating conditions. The list of the parameters used includes peak discharge current, peak axial velocity, axial transit time, duration of the radial collapse, pinch lifetime, and neutron yield. Also, the soft X-ray production was correlated with the neutron yield.

The data from discharges having the same peak current, same peak axial velocity, and comparable pinch lifetime, but different axial transit time, show that the neutron yield is higher for shorter duration of the axial phase. As the duration of the initial phases of the discharge, i.e. breakdown and lift-off phases, is included in our axial transit time, we infer that the breakdown phase could have a strong influence on the total neutron production. From discharges with the same peak current, same peak axial speed, and same axial transit time, but different pinch lifetime and duration of the radial collapse phase, we infer that a fast compression followed by a dynamical (with large time and space gradients) evolution during the pinch phase favours large neutron production. Another important feature that was observed is that, for the same peak current and same pinch lifetime, the neutron as well as the soft X-ray yields depend on the sheath velocity.

The evolution and dynamics of the plasma focus with composite anode geometry may be affected by the profile of the joint between the two sections of the inner electrode. It was observed during the preliminary experiments that

https://doi.org/10.1017/S0022377898006771 Published online by Cambridge University Press

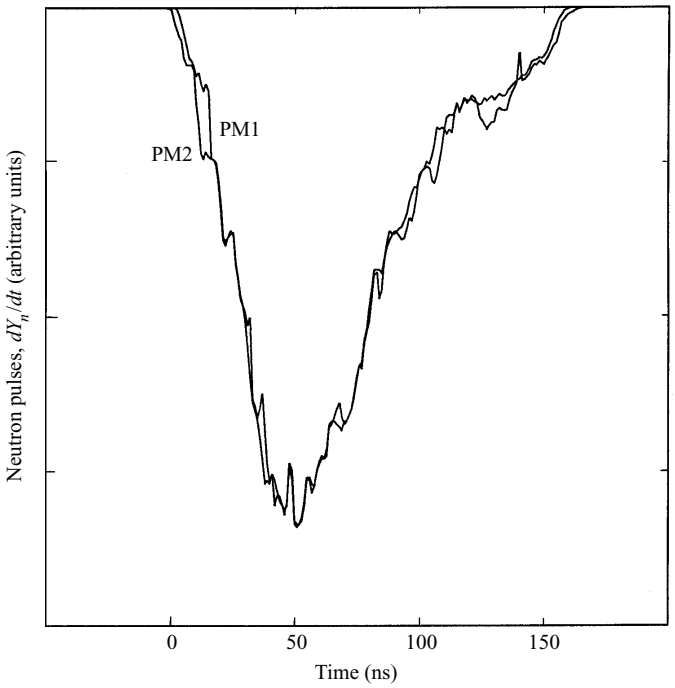


Figure 3. Neutron pulses obtained from the TOF detectors and compensated for their time of flight. Inner trace: signal from PM1. Outer trace: signal from PM2. Configuration: CCA-93/19+80/15. Discharge at 14 kV and 450 Pa D_2.

a steep joint aids the development of interchange instabilities. This may destroy the symmetry of the sheath even before the plasma enters the radial phase. Subsequently, the evolution and dynamics of the sheath during the final phase is affected. In order to avoid, or at least reduce, this effect, the profile of the joint has to be smooth and gradual.

Using the peak-to-peak method of analysis of the neutron pulses recorded with the two TOF detectors, an average energy of the neutrons emitted radially of 2.48 MeV was determined for all electrode configurations. Therefore the neutron pulses can be translated back in time according to their flight path. In this way, information on the neutron source was inferred. The result of this procedure is illustrated in Fig. 3. Each signal (from the near detector and far detector respectively) is normalized to the area under the trace, which is proportional to the total neutron yield. By overlapping the neutron signals, one can see the differences that appear at the beginning of the leading edge and the end of the trailing edge of the pulses due to neutron dispersion. Although proper TOF analysis and neutron spectroscopy were not performed because of our experimental limitations, we do not infer that the neutrons are monoenergetic.

On the basis of this result, we infer that the neutron emission commences at $t = 0(\pm 2$ ns). The time reference $t = 0$ is taken at the instant when the plasma column reaches the minimum radius at the end of the radial compression phase. The pinch lifetime t_p is defined as the duration from $t = 0$ to the instant corresponding to the development of the $m = 0$ instability. It was also observed that the neutron signal consists of two pulses, one emitted around $t = 0$ and the other at $t = t_p$, merged together owing to short values of the lifetime of the

https://doi.org/10.1017/S0022377898006771 Published online by Cambridge University Press

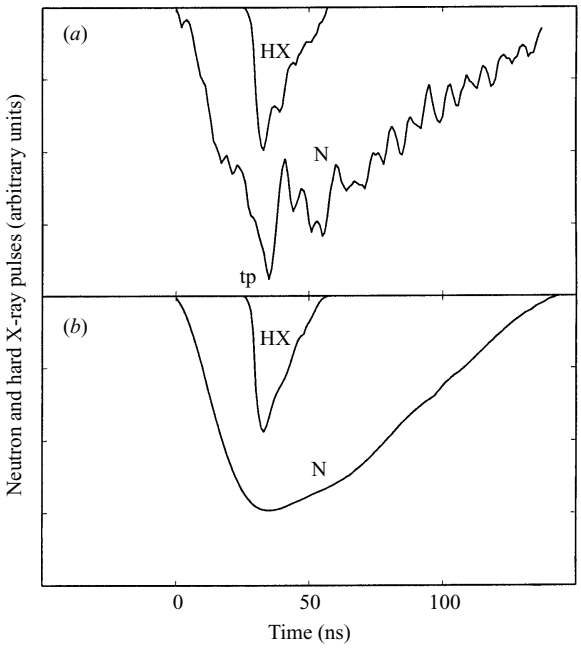


Figure 4. Time-resolved neutron (N) and hard X-ray (HX) pulses from the first TOF detector (PM1). The neutron pulse is compensated for its time of flight: (*a*) experimental data; (*b*) the corresponding pulses after smoothing. Configuration: CCA-103/19+70/15. Discharge at 14 kV and 450 Pa D_2.

pinch. Therefore one may estimate the number of neutrons emitted during the pinch lifetime by integrating the neutron signal dY_n/dt from $t = 0$ to $t = t_p$. In order to do so, the neutron signals from the TOF detectors have to be compensated for their flight path and overlapped with the hard X-ray pulses. Then the neutron signals (and eventually the hard X-ray signal) are smoothed using high-order polynomial functions. The procedure is illustrated in Fig. 4, where only the neutron signal recorded with the first TOF detector (PM1) is shown. The hard X-rays corresponding to the first plasma compression at $t = 0$ were cut off using lead sheets in front of the detector.

The results of this procedure give values of the percentage of the neutrons emitted during the lifetime of the pinch with respect to the total yield ranging between 4 % and 20 % for the neutron-optimized pressure of 450 Pa deuterium.

The plot of the average total neutron yield as a function of the fourth power of the peak discharge current illustrated in Fig. 5 shows that the neutron scaling law $Y_n \propto I^4$ does not hold exactly for all the electrode configurations tested in our experiments. The reason is that the neutron production mechanism(s) is affected by some factors such as force-field flow-field separation, electrode erosion or changes in the breakdown conditions. One could

(i) separate the neutron production into two components, i.e. a non-beam component such as the thermonuclear component Y_{th} and a beam–target component Y_{bt};

(ii) study the effect on these yield components of increasing the drive parameter and consequently the axial speed.

https://doi.org/10.1017/S0022377898006771 Published online by Cambridge University Press

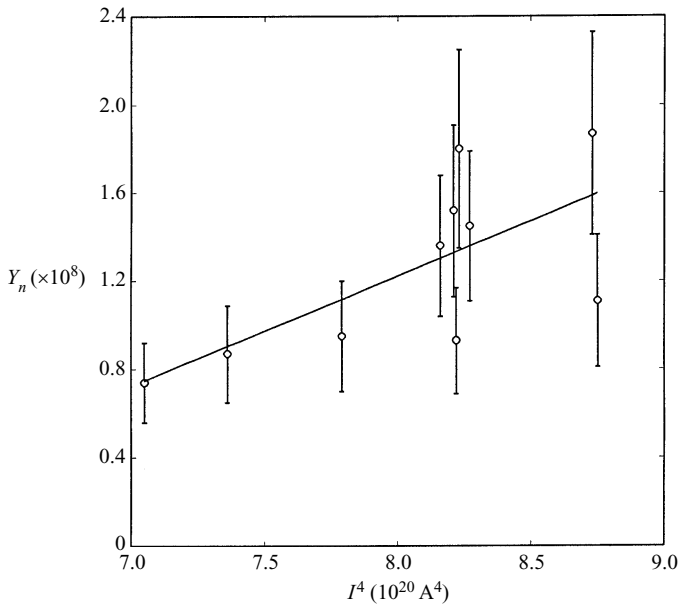


Figure 5. Total neutron yield as a function of the fourth power of the peak discharge current. The circles represent the mean values and the vertical error bars the corresponding standard deviations. Discharges at 14 kV and 450 Pa D_2.

In earlier experimental work (Chakrabarty 1988; Moo *et al.* 1991) on 3 kJ plasma focus devices, the reported value of the ratio $Y_{\rm th}/Y_{\rm bt}$ is of the order of 15/85. It has also been proposed (Lee 1994; Lee & Serban 1994) that the thermonuclear component can be written as follows:

$$Y_{\rm th} = CI_p^4\, v_{\rm axial}^4, \tag{1}$$

with C a constant over the range of plasma-focus devices.

We use our data to investigate whether our experiments verified (1).

The results obtained for a neutron-optimized pressure of 450 P deuterium are illustrated in Fig. 6. All data were included except those obtained from experiments with the electrode configuration OPA-185/15, CCA-45/19 + 140/15 and CCA-65/19 + 120/15. These were excluded because:

(i) the breakdown conditions were changed (OPA-185/15);

(ii) the speed-enhanced section of the anode was too long and led to force-field flow-field separation;

(iii) the reproducibility of the focus was very poor, thus affecting the mean value of the neutron yield.

The results (see Fig. 6) confirm that the data fit (1).

The value of the constant C in (1) was determined using a linear regression of the data plotted in Fig. 6: $C = 1.8 \times 10^{-34}$ (SI units). Thus (1) can be written in the form

$$Y_{\rm th} = 1.8 \times 10^{-6} I_p^4\, v_{\rm axial}^4 \qquad (\pm 30\,\%), \tag{2}$$

with I_p in kA and $v_{\rm axial}$ in cm μs^{-1} in the range of 7–14 cm μs^{-1}.

https://doi.org/10.1017/S0022377898006771 Published online by Cambridge University Press

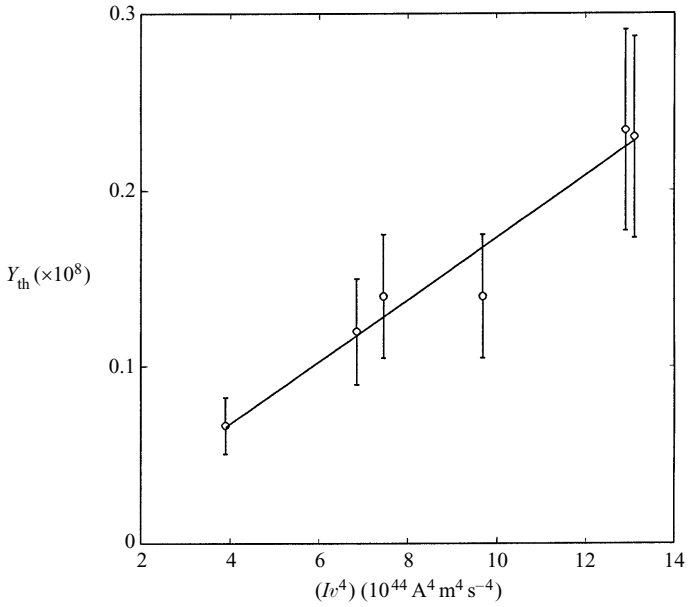


Figure 6. The non-beam component of the neutron yield as a function of $(Iv)^4$, where I is the peak discharge current and v is the peak axial speed. The circles represent the mean values and the vertical error bars the corresponding standard deviation. Discharges at 14 kV and 450 Pa D_2.

Table 3. Drive parameter $(I_p/a)\ p^{-1/2}$ and neutron yield at 450 Pa D_2.

Configuration	v_{axial} (cm μs^{-1})	I_{max} (kA)	$(I_{max}/a)\ p^{-1/2}$ (kA cm^{-1} (Torr D_2)$^{-1/2}$)	Y_n ($\times 10^8$)
SPF-165.19	8.3	172.0	97.8	1.11
OPA-175/17.5	9.5	171.9	106.2	1.87
OPA-180/17	9.7	169.9	108.1	1.36
OPA-185/15	10.4	162.1	116.8	0.73
CCA-45/19+140/15	10.5	164.7	118.7	0.87
CCA-65/19+120/15	10.6	167.1	120.5	0.95
CCA-103/19+70/15	11.2	169.4	122.1	1.80
CCA-93/19+80/15	11.3	169.5	122.2	1.50
CCA-90/19+100/15	—	169.6	122.3	1.45
CCA-95/19+90/14	11.4	169.4	130.8	0.95

Thus there is evidence within the limited range of our operation that the neutron yield of the plasma focus is enhanced by operating at higher speeds. We also have evidence that the X-ray production is also enhanced.

The values of the drive parameter and the corresponding neutron yield at 450 Pa deuterium filling pressure are listed in Table 3. It can be seen that there are two electrode configurations, namely OPA-175/17.5 and CCA-103/19+70/15, that produce, practically, the same neutron yield of approximately 1.8×10^8 neutrons/discharge. The increase of the drive parameter by 15% and of the axial speed by 17% for the CCA-103/19+70/15 geometry with respect to OPA-175/17.5 does not bring about an increase in the neutron output. One possibility is that, by operating the plasma focus at higher speed, the non-beam

https://doi.org/10.1017/S0022377898006771 Published online by Cambridge University Press

component of the neutron yield, such as that of thermonuclear origin, is enhanced (see (1)), while the beam–target component decreases according to the following expression (Lee 1994; Lee and Serban 1994);

$$Y_{\mathrm{bt}} = C' I_p^{4.5} v_{\mathrm{axial}}^{-1.5}, \tag{3}$$

where C' is a constant.

It is interesting to compare the performances of CCA-103/19 + 70/15 and CCA-93/19 + 80/15 as configurations of the same family of composite anodes. These two anodes have the same length and only a difference of 1 cm in the length of the speed-enhanced section. The configuration with the longer speed-enhanced section has a slightly higher speed, as expected. However, the neutron yield is reduced by 16 %. This degradation of neutron yield could be interpreted as the result of a significant separation of the shock front from the driving magnetic piston during the axial phase. Such a separation is proportional to distance travelled. It appears that increasing the speed-enhanced section from 7 cm to 8 cm results in an increase in that separation sufficient to affect the neutron yield. With sufficient separation, when the shock front is in radial motion, the magnetic piston is still moving axially. Therefore the radial compression is not driven or, if the separation is not too big, the efficiency of the drive is very poor, and leads to a low radiation yield.

A further increase in the length of the speed-enhanced section of the anode (see the data for the CCA-90/19 + 100/15 and CCA-95/19 + 90/14 anodes in Table 3) leads to a decrease in the total neutron yield. This is again consistent with the expected effect of force-field flow-field separation on the efficiency of the compression of the plasma column.

On the other hand, a comparison between the two high-neutron-output configurations, namely the OPA-175.17.5 and CCA-103/19 + 70/15 geometries, in terms of soft X-ray production shows that at higher speeds the soft X-ray emission is enhanced. A data analysis indicates that the plasma temperature during the pinch phase is higher. Assuming that the temperature T is proportional to the square of the velocity v, $T \propto v^2$ (Lee 1994), the temperature increases by almost 40 %. This is in agreement with the earlier interpretation of an enhanced non-beam neutron emission (Lee and Serban 1994).

The plasma focus device can be optimized for either neutron production or soft X-ray output. The optimization procedure has to meet conflicting requirements. An increase in the drive parameter by using a smaller-radius anode is favourable for increasing the plasma temperature, and thus the non-beam neutron component and the soft X-ray yield. At the same time, the pinch lifetime and dimensions are reduced accordingly (Lee and Serban 1996). Therefore the size of the radiation source is smaller. This effect is encouraging for practical applications of the plasma focus, for example as a soft X-ray source for lithography (Burkhalter *et al.* 1992).

4. Conclusions

Regardless of the electrode geometry, the neutron output of our plasma focus device has a strong dependence on the gas filling pressure. The neutron-optimized pressure is 450 Pa. The emission of neutrons begins at the end of the compression phase, when the plasma reaches its minimum radius.

https://doi.org/10.1017/S0022377898006771 Published online by Cambridge University Press

Peak axial sheath velocities of up to 15 cm μs^{-1} have been achieved (Serban 1995). The radiation output, i.e. both neutron and soft X-ray productions, increases as the speed increases. However, beyond a certain value of the peak axial speed and a certain length of the speed-enhanced section of the anode, the focusing characteristics and reproducibility are affected. We conclude that the length of the speed-enhanced section is critical. This section has to be long enough to increase the speed, but short enough to avoid the separation between the shock front and the magnetic piston. Also, the profile of the joint between the two sections of the anode plays an important role. An abrupt joint will favour the development and rapid growth of interchange instabilities, which will later affect the evolution of the focus during the final phases.

The results of the correlations of the neutron production and soft X-ray emission indicate that higher speeds enhance the temperature of the pinched column. The non-beam component of the neutron flux, taken to be of thermonuclear origin, is correlated with the peak discharge current and peak axial speed. A scaling law $Y_{\mathrm{th}} \propto (I_p v_{\mathrm{axial}})^4$ for the non-beam neutron component has been proposed on the basis of our experimental results within our range of operations. However, this scaling law should be checked with results from other plasma focus devices operating with a broader range of energies.

Acknowledgements

This work was performed with the help of Research Grant RP 9/94 LS. We also acknowledge contributions from Research Grant RP 29/92 VS.

References

Bernard, A., Bruzzone, H., Choi, P., Chuaqui, H., Gribkov, V., Herrera, J., Hirano, K., Krejci, A., Lee, S., Luo, C., Mezzetti, F., Sadowski, M., Schmidt, H., Ware, K., Wong, C. H. and Zoita, V. 1994 *Proposal Document for International Centre for Dense Magnetized Plasmas*. UNESCO.

Burkhalter, P. G., Mehlman, G., Newman, D. A., Krishnan, M. and Prasad, R. R. 1992 *Rev. Sci. Instrum.* **63**, 10.

Chakrabarty, C. K. 1988 MSc thesis, University of Malaya.

Conrads, H. 1992 *Laser and Plasma Applications* (ed. B. C. Tan), p. 120. Narosa, New Delhi.

Haines, M. G. 1982 *Physica Scripta* **T2/2**, 380.

Herold, H. 1990 *Proceedings of 3rd Tropical College on Applied Physics: Laser and Plasma Technology, 1988* (ed. C. S. Wong, S. Lee, B. C. Tan, A. C. Chew, K. S. Low and S. P. Moo), p. 21. World Scientific, Singapore.

Kies, W. 1988 *Proceedings of 2nd Tropical College on Applied Physics: Laser and Plasma Technology, 1986* (ed. S. Lee, B. C. Tan, C. S. Wong, A. C. Chew, K. S. Low, H. Ahmad and Y. H. Chen), p. 86. World Scientific, Singapore.

Lee, S. 1983 *J. Appl. Phys.* **54**, 3603.

Lee, S. 1988 *Proceedings of Energy Independence Conference, Rio de Janeiro, 1987: Fusion Energy and Plasma Physics* (ed. P. H. Sakanaka), p. 784. World Scientific, Singapore.

Lee, S. 1990 *Small Plasma Physics Experiments II* (ed. S. Lee and P. H. Sakanaka), p. 114. World Scientific, Singapore.

Lee, S. 1994 *Proceedings of International Conference on Plasma Science and Technology ICPST'94, Chengdu, China*, Paper D16, p. 137.

Lee, S. and Serban, A. 1994 *Proceedings of International Conference on Plasma Physics, ICPP'94, Foz Do Iguacu, Brazil*, Vol. 1, p. 181.

Lee, S. and Serban, A. 1996 *IEEE Trans. Plasma Sci.* **24**, 1101.

https://doi.org/10.1017/S0022377898006771 Published online by Cambridge University Press

Lee, S., Tou, T. Y., Moo, S. P., Eissa, M. A., Golap, A. V., Kwek, K. H., Mulyodrono, S., Smith, A. J., Suryadi, Usada, W. and Zakaullah, M. 1988 *Am. J. Phys.* **56**, 1.

Lee, S., Saw, S. H., Elfetouri, A. A., Shengher, A. N., Shummaki, E. O. and Hassan, N. A. 1991 *J. Fiz. Mal.* **12**, 25.

Moo, S. P., Chakrabarty, C. K. and Lee, S. 1991 *IEEE Trans. Plasma Sci.* **19**, 515.

Pouzo, J., Cortazer, D., Milanese, M., Moroso, R. and Piriz, R. 1988 *Small Plasma Physics Experiments* (ed. S. Lee and P. Sakanaka). World Scientific, Singapore.

Serban, A. 1995 PhD thesis, Nanyang Technological University, Singapore.

https://doi.org/10.1017/S0022377898006771 Published online by Cambridge University Press